

A novel particle time of flight diagnostic for measurements of shock- and compression-bang times in D3He and DT implosions at the NIF

H. G. Rinderknecht, M. Gatu Johnson, A. B. Zylstra, N. Sinenian, M. J. Rosenberg et al.

Citation: *Rev. Sci. Instrum.* **83**, 10D902 (2012); doi: 10.1063/1.4731000

View online: <http://dx.doi.org/10.1063/1.4731000>

View Table of Contents: <http://rsi.aip.org/resource/1/RSINAK/v83/i10>

Published by the [American Institute of Physics](#).

Related Articles

Temporally resolved plasma composition measurements by collective Thomson scattering in TEXTOR (invited)
[Rev. Sci. Instrum.](#) **83**, 10E307 (2012)

Impact of plasma noise on a direct thrust measurement system
[Rev. Sci. Instrum.](#) **83**, 033504 (2012)

A dual-channel, focusing x-ray spectrograph with uniform dispersion for Z pinch plasmas measurement
[Rev. Sci. Instrum.](#) **83**, 013106 (2012)

Cross-correlation based time delay estimation for turbulent flow velocity measurements: Statistical considerations
[Phys. Plasmas](#) **18**, 122304 (2011)

A novel zirconium K α imager for high energy density physics research
[Rev. Sci. Instrum.](#) **82**, 123503 (2011)

Additional information on Rev. Sci. Instrum.

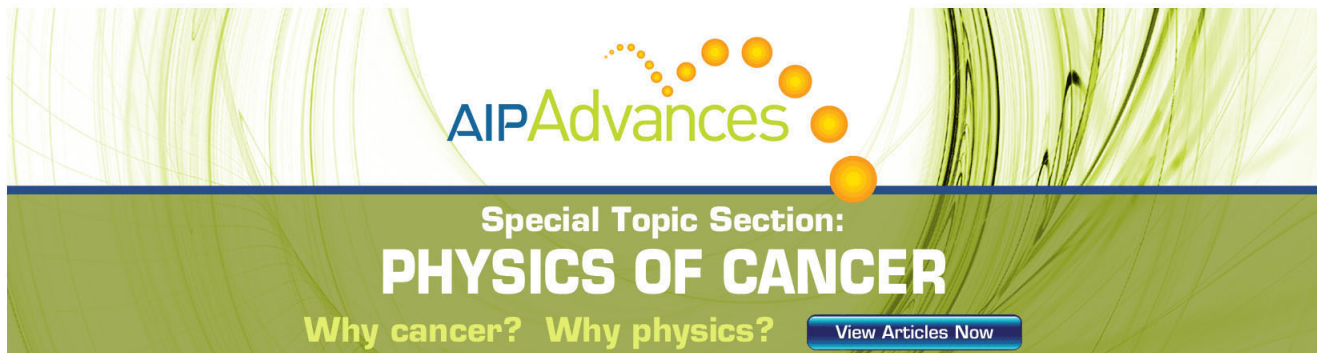
Journal Homepage: <http://rsi.aip.org>

Journal Information: http://rsi.aip.org/about/about_the_journal

Top downloads: http://rsi.aip.org/features/most_downloaded

Information for Authors: <http://rsi.aip.org/authors>

ADVERTISEMENT



AIP Advances

Special Topic Section:
PHYSICS OF CANCER

Why cancer? Why physics? [View Articles Now](#)

A novel particle time of flight diagnostic for measurements of shock- and compression-bang times in D³He and DT implosions at the NIF^{a)}

H. G. Rinderknecht,^{1,b)} M. Gatu Johnson,¹ A. B. Zylstra,¹ N. Sinenian,¹ M. J. Rosenberg,¹ J. A. Frenje,¹ C. J. Waugh,¹ C. K. Li,¹ F. H. Sèguin,¹ R. D. Petrasso,¹ J. R. Rygg,² J. R. Kimbrough,² A. MacPhee,² G. W. Collins,² D. Hicks,² A. Mackinnon,² P. Bell,² R. Bionta,² T. Clancy,² R. Zacharias,² T. Döppner,² H. S. Park,² S. LePape,² O. Landen,² N. Meezan,² E. I. Moses,² V. U. Glebov,³ C. Stoeckl,³ T. C. Sangster,³ R. Olson,⁴ J. Kline,⁵ and J. Kilkenny⁶

¹Massachusetts Institute of Technology, Cambridge, Massachusetts 02139, USA

²Lawrence Livermore National Laboratory, Livermore, California 94550, USA

³Laboratory for Laser Energetics, Rochester, New York 14623, USA

⁴Sandia National Laboratory, Albuquerque, New Mexico 87123, USA

⁵Los Alamos National Laboratory, Los Alamos, New Mexico 87545, USA

⁶General Atomics, San Diego, California 92121, USA

(Presented 8 May 2012; received 8 May 2012; accepted 30 May 2012; published online 2 July 2012)

The particle-time-of-flight (pTOF) diagnostic, fielded alongside a wedge range-filter (WRF) proton spectrometer, will provide an absolute timing for the shock-burn weighted ρR measurements that will validate the modeling of implosion dynamics at the National Ignition Facility (NIF). In the first phase of the project, pTOF has recorded accurate bang times in cryogenic DT, DT exploding pusher, and D³He implosions using DD or DT neutrons with an accuracy better than ± 70 ps. In the second phase of the project, a deflecting magnet will be incorporated into the pTOF design for simultaneous measurements of shock- and compression-bang times in D³He-filled surrogate implosions using D³He protons and DD-neutrons, respectively. © 2012 American Institute of Physics. [<http://dx.doi.org/10.1063/1.4731000>]

I. INTRODUCTION

Nuclear burn diagnostics¹ provide crucial information for understanding the physics of inertial confinement fusion² (ICF) experiments. In experiments at the National Ignition Facility (NIF),³ shocks launched into the ablator by the laser pulse are timed to coalesce within the gas fill.⁴ The combined shock rebounds from the capsule center, heating the shocked gas and causing a period of nuclear burn (“shock bang”) before compression by the imploding shell forms the hotspot (“compression burn”). The strength and timing of the combined shock are affected by target geometry, laser pulse, equations-of-state for the ablator and fuel, and preheat.⁵ A measurement of shock bang-time will guide understanding of the role of these components in the ignition campaign. In D³He-filled surrogate targets, the ρR at shock bang-time is determined from the wedge range filter (WRF) diagnostic.⁶ Measuring shock bang-time would greatly increase the value of this data by determining the ρR evolution of the capsule independent of simulations.

A chemical vapor deposition (CVD)-diamond-based detector⁷ is ideal for a novel measurement of the shock- and compression-bang times in implosions at the NIF. The detector is compact and vacuum-compatible, so it may be fielded close to the target to increase statistics and decrease time-of-flight uncertainty. A rapid detector rise-time allows timing ac-

curacy better than ± 50 ps. Furthermore, the ratio of detector sensitivity to protons and neutrons is comparable to the ratio of DD-neutron to D³He-proton yield in D³He-filled surrogate experiments at the NIF. Thus, the detector will simultaneously measure shock- and compression-bang time on a single diagnostic.

In this paper, the diagnostic design and implementation of pTOF at the NIF and data from the tuning campaigns in 2011 and 2012 are discussed.

II. EXPERIMENTAL SETUP

A particle time-of-flight (pTOF) diagnostic has been implemented to measure neutron bang-times at the NIF. An upgrade to the pTOF diagnostic is also being implemented for simultaneous and robust measurements of shock- and compression-bang times, using D³He-protons and DD-neutrons, respectively.

The pTOF detector is sensitive to impulses of energetic neutrons from the DT and DD fusion reactions (14.1 and 2.45 MeV, respectively), and protons from the D³He fusion reaction (14.7 MeV).⁸ A circular, synthetic diamond wafer made by the CVD technique is biased along its axis. Incident high-energy particles excite electron-hole pairs in the diamond volume, a fraction of which are collected by the bias field as a time-dependent current and recorded on an oscilloscope as a time-dependent voltage. The pTOF detectors are similar in operation to diamond-based neutron time-of-flight (nTOF) detectors at OMEGA and NIF (Ref. 9) and the south pole bang time system at NIF.¹⁰

^{a)}Contributed paper, published as part of the Proceedings of the 19th Topical Conference on High-Temperature Plasma Diagnostics, Monterey, California, May 2012.

^{b)}hgr@mit.edu.

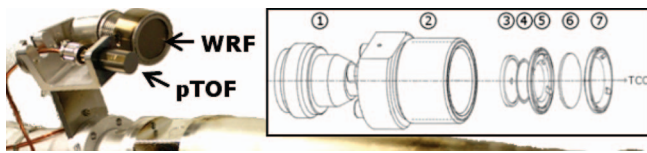


FIG. 1. The pTOF fielded with 2 cm W filtering on DIM (90,78), next to a WRF module. (inset) The pTOF detector consists of (1) N-type connector with biased pin, (2) brass housing, (3) ceramic insulator, (4) 200 μm thick, 10 mm diameter CVD-diamond wafer with electrodes, (5) grounding ring aperture (8 mm ID), (6) configurable filtering, and (7) filter cap.

The CVD-diamonds used are optical-quality, 200- μm thick samples with a diameter of 10 mm. The samples were acquired from Diamond Materials, GmbH,¹¹ and were further processed at Lawrence Livermore National Laboratory (LLNL), where electrodes were deposited on the front and rear surfaces. The 1 μm thick, 9 mm diameter Au electrodes were deposited on top of an intermediate 200 \AA Ti wetting layer. The diamonds are housed inside a brass assembly depicted in Fig. 1. A rear electrode pin biases the sample, which is grounded to the housing by a ring-shaped front aperture. The aperture leaves 64% of the detector surface exposed.

In the first phase of the pTOF implementation, the diagnostic is fielded on a diagnostic instrument manipulator (DIM) (Ref. 12) located at $(\theta = 90, \phi = 78)$ in the NIF chamber. The detector is biased at -250 V and fielded side-by-side with a WRF proton spectrometer.¹³ At 50 cm from target chamber center (TCC), pTOF is the closest nuclear bang-time diagnostic to TCC. Fig. 1 shows a snout assembly with pTOF.

X-ray signals, primarily generated by laser-plasma interactions, will dominate the DD-neutron and D^3He -proton signals for the pTOF detector at the NIF, if the detector is not properly shielded. To reduce the magnitude of the direct x-ray signal to the required level for accurate measurements of these species, a high-Z filter with an areal density of several tens of g/cm^2 is required. Such a filter stops any D^3He protons from reaching the detector. For this reason, the second phase of the pTOF implementation will include a permanent dipole magnet to deflect shock-bang protons onto the detector around a configurable line-of-sight filter with thickness ~ 2 cm.

Signals generated in the CVD diamond are transmitted from DIM (90,78) to the NIF mezzanine through 95 ft of low-loss LMR-400 cable. The signal is first recorded on an FTD10000 oscilloscope, then attenuated and split before it is recorded on two channels on a Tektronix DPO70604B digitizer. The FTD10000's ability to withstand large input voltages allows this two-scope configuration to record signal amplitudes between 1 mV and 250 V. A fiducial impulse signal, supplied by the NIF facility, provides a timing reference for both oscilloscopes. The cross-timing of the scope traces to the laser system is precise to within ± 15 ps.

III. ANALYSIS

For fusion neutrons, the source spectrum is well-approximated by a Gaussian distribution with a mean energy weakly dependent on ion temperature T_{ion} and width $\sigma \propto \sqrt{T_{ion}}$.⁸ For D^3He protons, the spectrum will be di-

TABLE I. Error budget for pTOF-measured bang times.

Source of uncertainty	Uncertainty
Crosstiming to laser system	± 15 ps
Detector IRF (<i>in situ</i>)	± 25 ps
Forward fit (S/N = 10)	± 18 ps
Cable repeatability shot-to-shot	± 5 ps
Nominal detector distance	± 0.5 mm \rightarrow
DT-n, DD-n, D^3He -p	± 10 ps, 23 ps, 12 ps
DIM positioning accuracy	± 1 mm \rightarrow
DT-n, DD-n, D^3He -p	± 19 ps, 46 ps, 23 ps
Magnet temporal broadening	± 5 ps (D^3He -p only)
Mean energy:	± 1 keV, 1 keV, 140 keV
DT-n, DD-n, D^3He -p	$\rightarrow \pm 1$ ps, 5 ps, 79 ps
Total: DT-n, DD-n, D^3He -p	± 41 ps, 62 ps, 90 ps

rectly measured by a WRF proton spectrometer located near the pTOF diagnostic.⁶ These source spectra are time-dispersed during flight to the pTOF detector to generate a signal source for the detector. In addition, the burn duration of an ICF implosion adds temporal broadening to the source function; typical burn durations at the NIF are ~ 150 ps FWHM.¹⁴

The source functions for nuclear particles are modeled with two independent variables: a mean time for nuclear production (bang-time), and an amplitude (yield). Proton and neutron source functions are scaled by the detector sensitivity to these particles. An arbitrary source function is generated in the x-ray signal region for background subtraction. The source functions are summed and convolved with the detector impulse response function (IRF) to generate a simulated pTOF signal, which is fit to the measured signal using a least-squares minimization algorithm to obtain nuclear bang times and yields.

The physics of this procedure is captured in the time-of-flight equation: $t_{bang} = t_{scope} - d/\beta c$. Uncertainty in the measured particle arrival time (t_{scope}), detector distance to the implosion (d), and particle velocity (β) contribute to the overall uncertainty in the bang-time measurement. For neutrons, as the mean energy is well known, uncertainty of the inferred bang-time is dominated by uncertainty in the detector distance. For D^3He protons, the mean energy uncertainty as measured by WRFs, typically 140 keV, will be the dominant source of uncertainty. See Table I for a summary of uncertainties.

IV. CALIBRATION

The IRF of the pTOF was determined *in situ* on the NIF. An 88 ps FWHM laser impulse incident on a silver foil was used on several occasions to generate a short burst of x-rays that drives an impulse into the pTOF system. On x-ray impulse shot N110531, the pTOF recorded an IRF characterized by a 370 ps rise and 1.70 ns FWHM. Such shots also supply an absolute timing calibration for the pTOF system relative

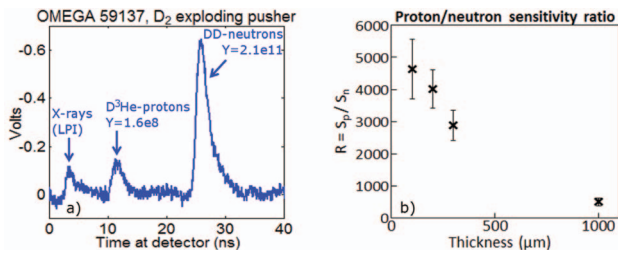


FIG. 2. pTOF calibration data recorded at OMEGA: (a) DD-exploding pusher, showing signals from x-rays, DD-neutrons, and secondary D³He-protons. This type of data was used to determine the pTOF sensitivity to fusion products. (b) Ratio of pTOF detector proton sensitivity to neutron sensitivity, as a function of detector thickness. Thinner detectors are observed to have higher relative proton sensitivity. Detectors were filtered with 100 μm Al + 100 μm Ta.

to the NIF laser. Uncertainty in the time-dependent spectral emission of the targets on such timing shots introduces a systematic uncertainty in the timing of the pTOF system of approximately ± 25 ps.

pTOF detectors have been fielded at OMEGA to determine sensitivity to nuclear products. A typical sensitivity of 2.0×10^{-8} V ns per incident 2.45-MeV-neutron, 5.4×10^{-8} V ns per incident 14.1-MeV-neutron, and 7.3×10^{-5} V ns per incident 6.5-MeV proton¹⁵ was observed in 200 μm thick diamonds at -250 V bias. The selection of pTOF diamonds have shown a range of sensitivity by factors of 0.5–4 around these values. Figure 2(a) shows an example of OMEGA calibration data.

The relative sensitivity of a detector to protons and to neutrons was found to vary as a function of the detector thickness. Figure 2(b) shows results from detectors between 100 and 1000 μm thick. Protons less than ~ 7 MeV will deposit their energy and stop in the first 200 μm of the diamond, while x-rays and neutrons both deposit energy volumetrically. Since x-ray and neutron sensitivity are expected to scale similarly, 200 μm detectors were chosen to optimize proton signal relative to background.

V. DATA

pTOF has recorded neutron data on over 70 NIF shots, including 22 cryogenic DT/THD shots, 7 DT exploding pushers, and 35 D³He gas-filled surrogate shots. An example of pTOF data from a recent cryogenic DT shot is shown in Fig. 3(a). The pTOF-measured DT-neutron bang times agree with the nuclear bang-time measured by GRH,¹⁴ given the uncertainties involved. Figure 3(b) shows pTOF vs GRH-measured nuclear bang-times.

Bang-times measured with DD-neutrons on D³He surrogate shots are also in agreement with x-ray bang-time measurements; however, large x-ray backgrounds have reduced the accuracy of that measurement to $\sim \pm 200$ ps. Recently, 2 cm W filtering has been fielded which reduces the x-ray signal to the same order as DD-neutron signals, allowing accurate bang-time measurements.

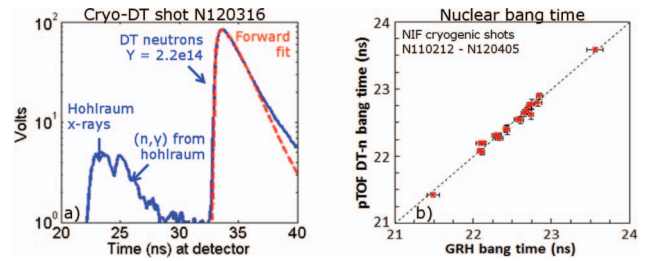


FIG. 3. pTOF data recorded at the NIF: (a) Cryogenic DT shot, showing signals from x-rays, DT-neutrons, and (n,γ) reactions in the hohlraum. Detector filtering was 1 mm Ta. The best fit to the DT-neutron peak is overplotted. (b) Nuclear bang-times measured with pTOF agree with measurements from the gamma reaction history diagnostic (GRH) to within experimental uncertainties ($\chi^2_{reduced} = 0.64$).

VI. CONCLUSIONS

A novel diagnostic for measuring shock and compression bang-times has been calibrated at OMEGA and designed and implemented at the NIF. The pTOF diagnostic reports absolute bang-times using DT-neutrons and DD-neutrons. Results support the ongoing design of the magnet-based pTOF, for which expected signals on D³He surrogate shots are ~ 200 mV for D³He-protons, ~ 100 mV for DD-neutrons, and less than 500 mV from x-rays. This instrument will simultaneously provide the first robust measurements of shock- and compression-bang time on surrogate D³He-filled implosions at the NIF.

ACKNOWLEDGMENTS

The authors thank the engineering and operations staff at NIF, LLE, and MIT for their support. This work performed under the auspices of the U.S. Department of Energy (DOE) by Lawrence Livermore National Laboratory under Contract No. DE-AC52-07NA27344. This work was done in part for H. Rinderknecht's Ph.D. thesis and was supported in part by the U.S. DOE (DE-FG52-09NA29553), LLNL (B580243), LLE (414090-G), the Fusion Science Center at the University of Rochester (415023-G), and the National Laser Users Facility (DE-NA0000877).

¹V. Y. Glebov *et al.*, *Rev. Sci. Instrum.* **77**, 10E715 (2006).

²S. Atzeni and J. M. ter Vehn, *The Physics of Inertial Fusion* (Oxford University Press, 2004).

³E. I. Moses, *Fusion Sci. Technol.* **44**, 11 (2003).

⁴T. R. Boehly *et al.*, *Phys. Plasmas* **16**, 056302 (2009).

⁵R. E. Olson *et al.*, *Bull. Am. Phys. Soc.* **56**, CO8.00003 (2011).

⁶A. B. Zylstra *et al.*, "Charged-particle spectroscopy for diagnosing shock ρR and strength in NIF implosions," *Rev. Sci. Instrum.* (these proceedings).

⁷G. J. Schmid *et al.*, *Rev. Sci. Instrum.* **74**, 1828 (2003).

⁸L. Ballabio, J. Källne, and G. Gorini, *Nucl. Fusion* **38**, 1723 (1998).

⁹V. Y. Glebov *et al.*, *Rev. Sci. Instrum.* **81**, 10D325 (2010).

¹⁰A. G. MacPhee *et al.*, *J. INSTRUM* **6**, P02009 (2011).

¹¹See <http://www.diamond-materials.com/> for more information.

¹²W. J. Hibbard, M. D. Landon, M. D. Vergino, F. D. Lee, and J. A. Chael, *Rev. Sci. Instrum.* **72**, 530 (2001).

¹³F. H. Séguin *et al.*, *Rev. Sci. Instrum.* **74**, 975 (2003).

¹⁴H. Herrmann *et al.*, *J. Phys.: Conf. Ser.* **244**, 032047 (2010).

¹⁵D³He protons were ranged down to stop in the 200-μm detector.